ELSEVIER

Journal of Contaminant Hydrology 22 (1996) 39–66

JOURNAL OF
Contaminant
Hydrology

Effects of high variance of fracture transmissivity on transport and sorption at different scales in a discrete model for fractured rocks

A. Wille Nordqvist [a], Yvonne W. Tsang [b], Chin-Fu Tsang [b], Björn Dverstorp [c], Johan Andersson [c]

[a] *Hydraulics Engineering, The Royal Institute of Technology, S-100 44 Stockholm, Sweden*
[b] *Earth Sciences Division, Lawrence Berkeley Laboratory, University of California, Berkeley, CA 94720, USA*
[c] *Swedish Nuclear Power Inspectorate, S-106 58 Stockholm, Sweden*

Received 23 January 1995; accepted 31 May 1995

Abstract

A three-dimensional (3-D) variable-aperture fracture network model for flow and transport in fractured crystalline rocks has been applied to study the effects of large variability in fracture transmissivity on non-sorbing and sorbing tracer transport, and scale effects in transport distance. The variable-aperture character of the fractures is introduced into a 3-D network model through a library of single-fracture permeabilities and associated particle transport residence time spectra. Sorption onto the fracture walls is added by a mathematical model for linear sorption. The resulting variable-aperture fracture network model, VAPFRAC, can handle flow and transport from single-fracture scale to the multiple-fracture scale. The model produces multi-peak transport breakthrough curves even for relatively moderate values of the fracture transmissivity variance. These breakthrough curves display dispersion on two different scales in the same way as has been observed in several field experiments conducted in crystalline rocks. The multi-peak structure is due to so-called channeling. For high values of the fracture transmissivity variance the solute transport is unevenly distributed and the channeling effects are more prominent.

The effect of linear sorption is not just a simple translation in mean residence time as in a homogeneous medium. The dispersion characteristics of the breakthrough curves also change when linear sorption is included. The degree of the change depends strongly on the fracture transmissivity variance, as does the translation. In particular, with a high fracture transmissivity variance the translation in mean residence time due to sorption is significantly smaller compared to the cases with a low fracture transmissivity variance. Finally, the high variability in the model output data suggests that extrapolation of results from a particular tracer experiment will be highly uncertain.

SSDI 0169-7722(95)00064-X

1. Introduction

At present there is considerable interest in fluid flow and solute transport in fractured crystalline bed-rock. This stems not only from concern with contaminant transport in the subsurface, but also from the safety assessment of geologic repositories for deep disposal of highly radioactive nuclear wastes. The advective transport in the fractures together with the ability for sorption on the fracture walls and diffusion into the rock matrix are some of the important phenomena controlling the movement of toxic agents or radioactive nuclides.

Field experiments in fractured rocks show that only a limited part of the volume within the fractures is open to fluid flow and solute transport. This part, that might be as small as $\leq 10\%$ of the fracture volume (Moreno et al., 1988), consists of tortuous flow paths in the plane of the fractures. The tortuosity arises from a high variance in fracture aperture over the fracture planes. Quite contrary to this fact, many existing discrete models for flow and transport in fractured media assume that flow occurs in the entire plane of the fractures (e.g., Long et al., 1985; Robinson, 1986; Andersson and Dverstorp, 1987), or in tubes imbedded within the fracture planes (e.g., Neretnieks et al., 1982; Rasmuson and Neretnieks, 1986; Tsang and Tsang, 1987; Cacas et al., 1990a, b; Dverstorp et al., 1991; Moreno and Neretnieks, 1993a, b). In these models the permeability is constant over each fracture plane or along each tube. This is in fact not the case in the field. Instead the resistance to flow may differ several orders of magnitude in different parts of the same fracture due to the variation in fracture aperture (Abelin et al., 1989).

Several comprehensive field studies of fluid flow and tracer transport on multiple-fracture scale have been performed in crystalline rocks (e.g., Abelin and Birgersson, 1987; Abelin et al., 1987a, b; Cacas et al., 1990a, b; Gale et al., 1990a, b; Holmes et al., 1990; Black et al., 1991; Wikberg et al., 1991). They all indicated a large degree of heterogeneity giving rise to a concentration of fluid flow to preferential paths. This effect, called flow channeling, manifests itself in the coalescence of transported particles to a few dominating routes throughout the network of fractures in the rock.

In order to account for the effects of dynamic flow paths induced by the aperture variation within each fracture a variable-aperture fracture network model (VAPFRAC) (Nordqvist et al., 1992) was developed. The introduction of variable apertures in the fractures of a random network is a new approach to modeling flow and transport in fractured rock. It explicitly accounts for both tortuous flow paths within the individual fractures, resulting in a spectrum of possible fracture residence times, and flow channeling on the multiple-fracture scale. To our knowledge, this way of combining the effects of transit time variation within the fractures with the complexity and randomness of a fracture network is novel.

A considerable portion of research has focused on understanding the transport behavior not only in discrete media but also in heterogeneous porous media. A strong motivation for this research has been discrepancies between field-scale and laboratory observations (e.g., Ptacek and Gillham, 1992; Kent et al., 1994). The framework for the modeling of reactive subsurface transport taking random heterogeneity of physical and chemical properties into account was described by Cvetkovic (1996). According to him,

the discrepancy between field and laboratory reaction parameters may be a result of their spatial variability and of the different mixing, due to heterogeneity, in the field and in the laboratory.

In a comprehensive study by Burr et al. (1994) the field-scale transport of reactive and non-reactive solutes by groundwater in a statistically anisotropic aquifer was examined by means of numerical solutions of the steady-state flow and transient advection–dispersion equations, in three dimensions. The physical and chemical heterogeneities were modeled with the use of geostatistical descriptions of the hydraulic conductivity field and the field of the chemical distribution coefficient, inversely correlated to each other. Their analysis showed that the ensemble mean bulk retardation factor can increase with time, even though the sorption is linear and instantaneous and the flow field is steady state.

The main objective of this study is to present a model that constitutes a reasonable and physically more realistic alternative to the classical continuum approach for describing transport in highly heterogeneous fractured rock. A novel detailed representation of fractured rock heterogeneities in the discrete model allows us to:

(1) analyse how heterogeneities on different scales in fractured rock affect solute transport;

(2) illustrate transport distance scaling properties in fractured media;

(3) quantify the effects on the sorption process of fractured rock heterogeneities.

2. Model description

The variable-aperture fracture network model (VAPFRAC) is described in detail in Nordqvist et al. (1992) and will be summarized here. It has its origin in two models developed previously. The first is the fracture network model (DISCFRAC) (Andersson and Dverstorp, 1987) which models fractured rocks as a network of circular discs (fractures). The second is the variable-aperture fracture model (Moreno et al., 1988) which represents single fractures as a two-dimensional (2-D) field of varying apertures. The basic concept, illustrated in Fig. 1, of how the two models are combined is to start by calculating flow and transport characteristics for single fractures. The results are then used as input for running particles through a network of fractures (see the following).

First, flow and transport characteristics through single fractures with unit length and unit width are computed. Each fracture plane is discretized into equally sized square elements (grid blocks). Aperture values are generated by geostatistical methods and then assigned one to each grid block. The flow between adjacent grid blocks is controlled by local permeabilities which are proportional to the square of the apertures in the grid blocks. A hydraulic head difference equal to unity is applied in one direction over each unit fracture (the other two boundaries are closed), resulting in a system of linear equations, the solution of which yields the hydraulic head at the center of each grid block. The hydraulic head differences between adjacent grid blocks multiplied by the local permeabilities give the local flow rates. The total flow through the unit fracture, obtained by adding all the local flows along an open boundary, divided by the hydraulic head difference over the fracture yields the all effective transmissivity for the entire

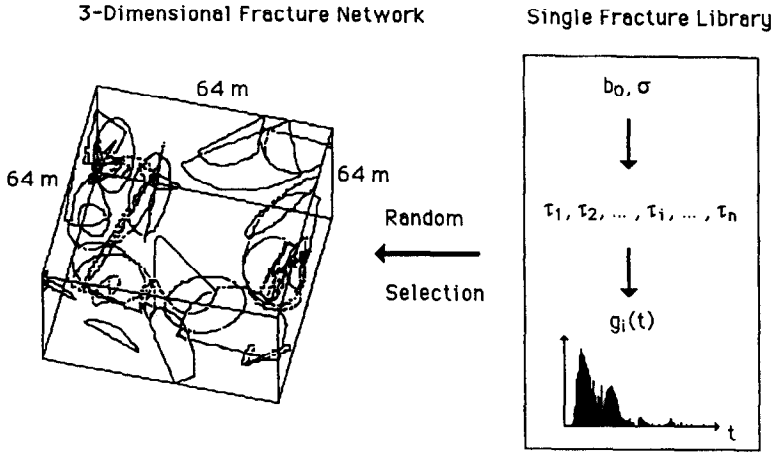

Fig. 1. Illustration of the basic concept of how the variable-aperture fractures are introduced into the fracture network model (see text for explanation).

fracture. Finally, a particle tracking technique is employed to calculate a distribution of transit times for transport of particles through each fracture. At each grid block the particles choose travel directions in proportion to the flow rates to the neighbouring grid blocks. The residence time at each step is derived from the flow and volume in the grid block. The fracture transit times and their probabilities thus obtained are recorded as time spectra. In this manner, one obtains an effective transmissivity, τ_i, and a residence time spectrum, $g_i(t)$ characterizing the flow and transport properties of each realization of a single fracture. The compilation of these residence time spectra with their corresponding effective transmissivities for many single fractures constitute the so-called single-fracture library.

Because of the mixing in the grid blocks, there is no need for an artificial model for dispersion to be incorporated in the VAPFRAC model. The numerical solution of the particle tracking algorithm within the fracture plane is controlled such that the effective transverse dispersion reflects the physical flow distribution in the plane [for more details see Moreno et al. (1991)].

At fracture centers, particles select new flow directions weighted on the out-going flux as described below. This mixing also introduces local transverse dispersion in contrast to a situation with perfect correlation between flow paths in different fracture planes. Due to lack of more detailed information from the field, there are several conceivable concepts for the modeling of these mixing processes. Although the present mixing concept is thought to be a reasonable approximation of the true flow and transport behavior in a fractured medium, this is indeed a conceptual uncertainty that deserves further investigation.

The library fractures generated by the variable-aperture fracture model are randomly assigned to the fractures in the three-dimensional (3-D) network generated by the DISCFRAC model. The actual geometry, i.e. length and width, of the fractures in the network modifies the effective transmissivities from the library fractures assuming that

the transmissivity is linearly dependent of fracture intersection width and inversely proportional to transport distance within the fractures of the network. A hydraulic head difference is then applied in one direction over the entire network. The four sides of the flow domain parallel to the hydraulic head gradient are no-flow boundaries. Knowing the boundary hydraulic head values the fracture transmissivities are used to set up a system of linear equations. The solution of these equations yields the hydraulic head values at all the fracture intersections. The differences between hydraulic heads at adjacent intersections and the corresponding fracture transmissivities then give the fluid flow rate of all the fractures in the network.

Proceeding to calculations of transport through the network, the particles are introduced on the up-stream boundary surface and collected on the down-stream boundary surface. The flow solution determines the travel routes of the particles transported through the network. At fracture centers complete mixing occurs. Accordingly if three or more fractures intersect a certain fracture the probability of a particle leaving the center of the fracture towards one of the intersecting fractures is proportional to the flux in that direction.

The residence time spectra in the single-fracture library are utilized for the calculation of total network transit times as follows. When a particle travels through the fractures of a network, fracture residence times are randomly drawn, in proportion to their probability, from the time spectrum of the corresponding library fracture. The library fractures are all 1 m long whereas the transport sections, between the fracture centers and fracture intersections (or the boundaries), within the fractures of the network may take on any

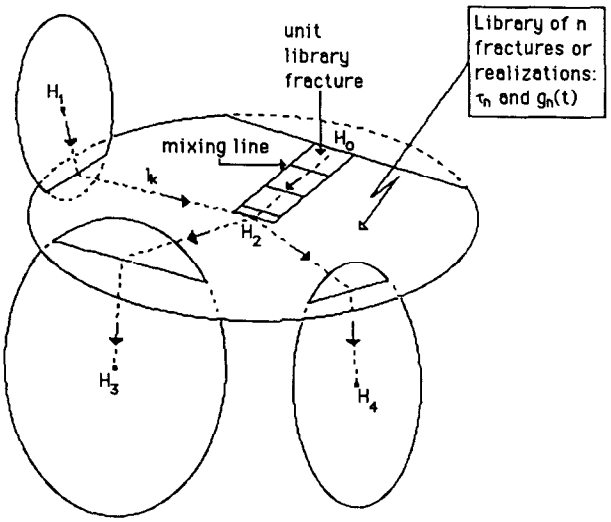

Fig. 2. A representation of how the variable-aperture fractures are inserted within the circular fractures in the network. The square elements along one of the sections illustrate how the single fracture from the library is repeatedly used in the calculations of the residence time for a transport section in the network. l_k is the distance of a transport section from the fracture center to an intersection or to the boundary. The hydraulic head values are denoted H_i ($i = 1, \ldots, 4$).

length l_k (in Fig. 2). Therefore, when the transport time of a section is calculated, the section is divided into unit lengths. For each such length a transport time is drawn from the library fracture that corresponds to the network fracture in question (see Fig. 2). The sum of these transport times gives the total residence time of the transport section.

Numerical analyses of tracer injection in single fractures show that mixing between fast and slow flow paths indeed occurs (e.g., Moreno and Tsang, 1991). Even if the up-scaling method, that is used in the present model to obtain the residence time of a transport section, may exaggerate this mixing within the fractures, the results of Moreno and Tsang clearly demonstrate that it would not be correct to neglect it altogether by scaling of only one time from the library.

The actual pressure drop of each fracture in the network modifies the fracture residence time from the library assuming that the fracture residence time depends linearly on the pressure drop over the fracture. The sum of all residence times of the network fractures that a particle has travelled through is the total residence time for transport from one boundary of the network to the opposite one. Repeating this procedure for a large number of particles makes it possible to plot mass transport breakthrough curves.

Thus, the output data of the VAPFRAC model consist of fluid flow rate, mass transfer residence times and spatial distribution of mass. The mass transfer results are converted into transport breakthrough curves characterized by first arrival time, mean time, dispersion in time and space, and number of peaks. These parameters comprise important information about the mass transport.

3. Linear sorption

The model described above is extended in the present study to incorporate sorption of tracer on fracture walls. This surface reaction is instantaneous and reversible and there is a linear relation between the concentration in the fluid and on the solid surface. The effect is included in the variable-aperture fracture network model by:

$$t_{i,s} = t_i \left\{ 1 + \frac{2K_a}{b_i} \right\} \tag{1a}$$

where $t_{i,s}$ and t_i are the residence times in a grid block with and without linear sorption, respectively; b_i is the grid block aperture; and K_a is the surface equilibrium constant given by:

$$K_a = K_d \rho_m \delta \tag{1b}$$

[K_d is the surface distribution coefficient; ρ_m the bulk density of the rock matrix; and d the "depth" of surface sorption (SKI, 1991)]. The expression within brackets in Eq. 1a is the surface retardation coefficient and can be derived directly from the one-dimensional (1-D) advective–dispersive equation with sorption onto the fracture surface (see, e.g., Neretnieks et al., 1982 or Moreno et al., 1985). It is a multiplicative correction of the residence times in each grid block of the variable-aperture fields and accounts for delay due to sorption onto the fracture surface, not accounting for the details of the

chemistry that is involved. This linear sorption model is introduced when constructing residence time spectra for the library fractures.

Thus, without sorption, the residence time within each grid block of the single fractures is given by:

$$t_i = \frac{Ab_i}{q_i} \tag{2}$$

and with linear sorption it is given by:

$$t_{i,s} = \frac{Ab_i}{q_i}\left\{1 + \frac{2K_a}{b_i}\right\} = \frac{A}{q_i}\{b_i + 2K_a\} \tag{3}$$

using Eq. 1a. A is the grid block area parallel to the flow direction and q_i the volumetric flow rate in grid block i.

For a vast majority of the grid block apertures from the aperture distributions of this study, K_a is much larger than b_i for most radionuclides of nuclear waste. Therefore, an approximate relation between grid block residence times with and without linear sorption for a specific grid block is:

$$\frac{t_{i,s}}{t_i} \cong \frac{2K_a}{b_i} \tag{4}$$

This implies that the grid block aperture has a direct influence on the time delay in the grid block. From Eq. 4 it is evident that a small variation in grid block aperture implies that sorption is just a translation in residence times, but that this is not necessarily the case when the aperture varies considerably between grid blocks.

4. Model parameters

The various statistical distributions in the single fracture and network-generating parts of the model require a set of parameters. Table 1 lists the distributions, their parameters

Table 1
Fracture network parameters

	Distribution	Parameter
Fracture radius [a], r	exponential	$\mu_r = 2.3$ m
Fracture center density [a], λ	Poisson space process 4s $i = 1, \ldots, 4$ (no. of fracture set)	$\lambda_i = 0.0018$–0.018 m^{-3},
Facture orientation [a], (θ,Φ)	Fisher distribution (Mardia, 1972) fitted to each of three roughly orthogonal (one subhorizontal and two subvertical) fracture sets and one random orientation set	
Fracture aperture, b	log normal	$b_0 = 10$ μm, $\sigma = 0.43$, 1.17

[a] Obtained from analysis of Stripa-3D experiment (Dverstorp et al., 1991).

Table 2
Some fracture aperture values from different field experiments and modelling work

Aperture (μm)	Type or object of study	Authors
60	effective aperture, hydraulic interface tests	Novakowski et al. (1985a)
510	effective aperture, tracer tests	Novakowski et al. (1985b)
80	model parameter	Tsang and Tsang (1987)
240	experimental value	Tsang and Tsang (1987)
15–190	hydraulic interference tests	Raven et al. (1988)
4	Stripa granite	Stratford et al. (1990)
0.6–670	Stripa granite	Tsang et al. (1991)
800	experimental value, drill cores	Hakami and Stephansson (1993)

and the range of values that were used in the present work. Field studies have guided the choices of distributions and parameters according to the following.

In order to generate fracture density, fracture radii and fracture orientations the model uses distributions and parameters that are based on an analysis (Dverstorp and Andersson, 1989; Dverstorp, 1991) of flow and transport data from the Stripa-3D experiment (Abelin and Birgersson, 1987; Abelin et al., 1987a, b) in Sweden. For the fracture network this results in a fracture spacing on the order of 1–3 m.

There is, of course, a large uncertainty related to how to describe the local variation within the individual fractures. Field experiments carried out in single fractures (Bourke et al., 1985) and measurements of aperture values in laboratory core samples (Gentier, 1986; Gale, 1987; Cox et al., 1989) and in transparent replicas of fractures (Hakami and Barton, 1990) indicate that the fracture apertures are consistent with a log normal distribution. Hence, a log normal distribution is used when generating fracture aperture values for the grid blocks of the single fractures in the library. The arithmetic mean of the fracture aperture is calibrated on the measured flow rate at Stripa to result in values of 18 μm in the case of low variance in fracture transmissivity and 280 μm in the case of high variance (see below). For comparison with aperture estimates from field experiments and modeling work see Table 2. The assumption of a log normal distribution for the fracture aperture implies that the fracture transmissivity of generated fracture realizations also obey a log normal distribution (Nordqvist et al., 1992). Field studies support a log normal distribution for the fracture transmissivity (Bourke et al., 1985; Cacas et al., 1990a). With the parameters b_0 and σ (Tsang et al., 1988) from Table 1 used for the generation of fracture block grid apertures, the fracture transmissivity of the fracture realizations has a mean log value, $\mu_{\ln T}$, of -22 and a standard deviation, $\sigma_{\ln T}$, of 1.5 or 3.1 on the natural logarithmic scale. The two different values of fracture transmissivity variance are obtained with the aperture generation parameter σ of the standard deviation in log aperture equal to 0.43 and 1.17, respectively. The spatial correlation length is 0.4 of the library fracture side. Investigations of fracture transmissivities in crystalline rock give values of $\sigma_{\ln T}$ between 2 and 8 on a natural logarithmic scale (Moreno and Neretnieks, 1993b). Specifically, Dverstorp et al. (1991) indicated that a $\sigma_{\ln T}$ of ~ 4 probably is representative for the fractured rock at Stripa. However,

the usage of two values in this study illustrates how the variability of the fracture transmissivity affects the transport simulation results.

The constant surface distribution coefficient, K_a, in Eq. 1a, for the linear sorption runs is 270,000 μm which is obtained with K_d equal to 1 m^3/kg, ρ_m equal to 2,700 kg/m^3 and δ equal to 10^{-4} m in Eq. 1b. These values, based on McKinley and Scholtis (1991) and SKI (1991), are typical for some important radioactive elements such as Pu and Am.

The flow and transport properties of the flow network under study are independent of library size when a library of ~ 100 or more fractures is used. It is accordingly not necessary to generate a new library fracture for each network fracture. The present model utilizes a fracture library consisting of 150 single fractures for each combination of b_0 and σ. For the fracture parameters of Table 1 and a flow domain of $64 \times 64 \times 64$ m^3 used in this work, there is on the average 8600 fractures in each realization. This entails that each spectrum in the library contributes with a fracture residence time ~ 60 times for every network simulation.

5. Transport simulation procedure

The flow domain is cubic with the side equal to 64 m. The fractures, however, were generated in a much larger volume in order to avoid a lower fracture density close to the boundaries of the flow domain. The hydraulic head difference in one direction over the flow domain was 1 m/m. Scaling of the hydraulic head difference easily produces flow and transport results for different gradients. The particles were introduced in the most conductive fracture intersecting within an area of 100 m^2 in the center of the up-stream vertical surface. This is meant to imitate the methods used in the field when tracers are injected in borehole sections where there are large local permeabilities. Particle input within a central area of the surface also minimizes the influence of the four no-flow boundaries parallel to the flow direction. The particles were collected over the entire down-stream vertical surface where their total transport times and positions were registered. Intermediate particle transport times and positions were registered at observation planes cutting through the entire flow domain perpendicularly to the mean flow direction at every 4 m.

Flow and transport simulations were performed for a low and a high value of the variance in fracture aperture and for a non-sorbing and a sorbing tracer. For each of these four calculation cases, an ensemble of 12 realizations of fracture networks were analyzed. The mean fracture aperture was adjusted to give the same mean flow rate for both values of aperture variance. In this way, the ensembles are different with regard to the variance of the fracture aperture (low and high) and the nature of the transported solute (non-reactive and reactive), only. The geometry of the networks is identical in corresponding realizations of different ensembles, but, for obvious reasons, different for the realizations within each ensemble. Although only 12 realizations were considered for each combination of input parameters in the analysis, this number is believed to be sufficient to acquire reasonably reliable information on the trends of the transport behavior. The reliability of the results presented here has been explored by a comparison

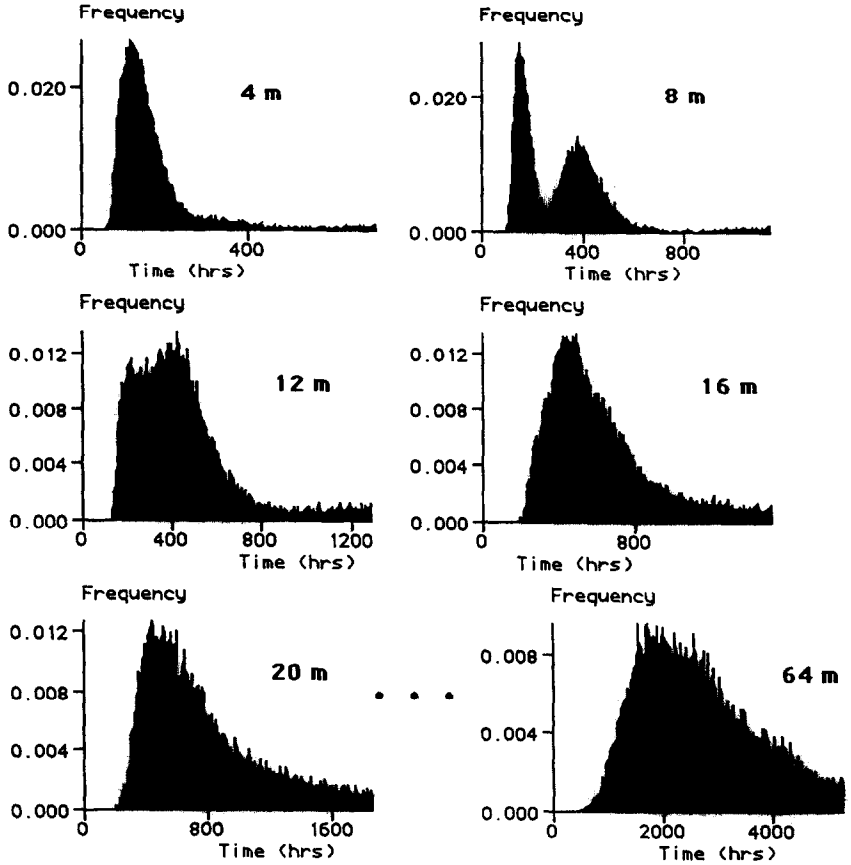

Fig. 3. A typical series of transport breakthrough curves for one realization showing relative frequency of particles vs. transport time for different distances from the source. The side of the network is 64 m and the input parameters are according to Table 1 with the low value of σ.

to the results of another set of ensembles of 12 realizations. Essentially identical results were obtained.

6. Transport simulation results

6.1. General characteristics of mass breakthrough

Figs. 3–6 display four typical series of mass breakthrough curves for a non-sorbing tracer. Each figure contains breakthrough curves recorded at different distances from the source. Figs. 3 and 4 are results for two realizations of fracture networks with the low variance of fracture aperture (fracture transmissivity). Figs. 5 and 6 display breakthrough curves with the high value of the aperture variance. An inspection of all series of

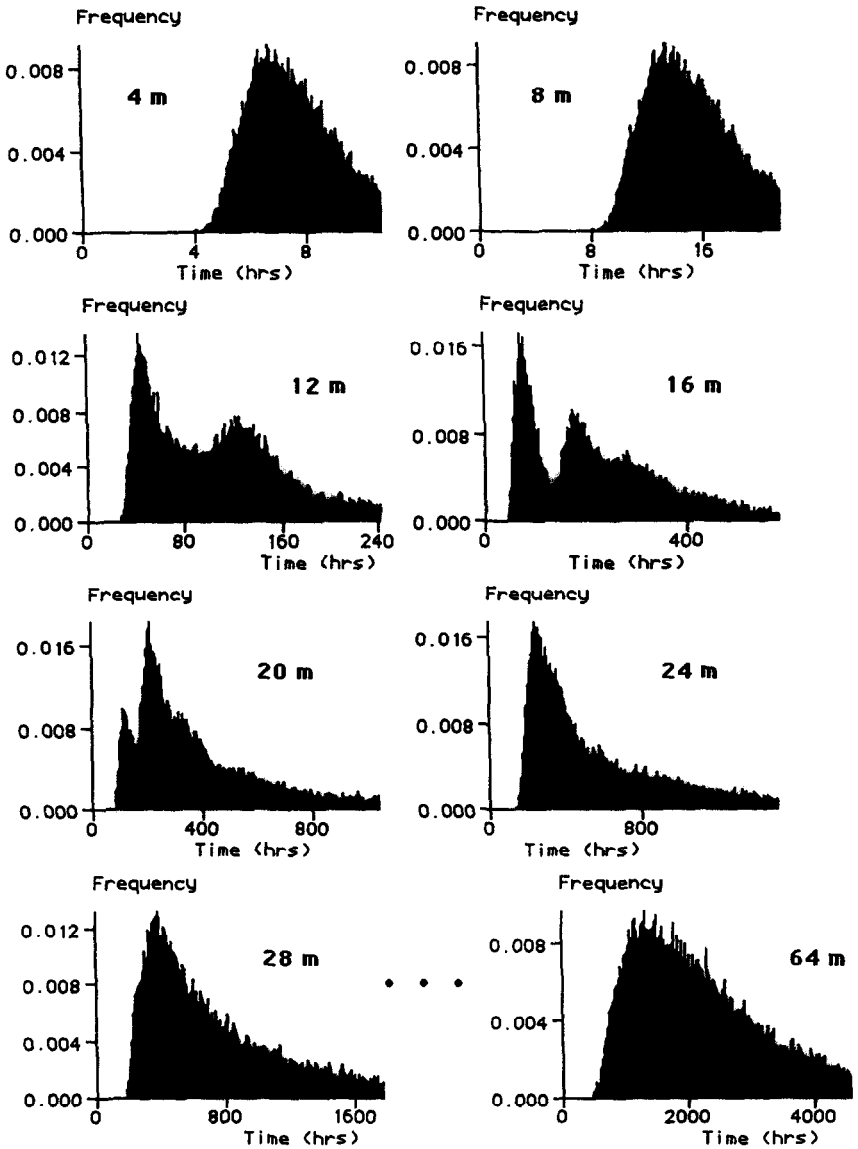

Fig. 4. A typical series of transport breakthrough curves for another realization with the same input parameters as in Fig. 3.

breakthrough curves leads to the following inferences. First, for the high value of the fracture transmissivity variance the positive skewness of the curves is more pronounced with a tendency towards relatively faster initial breakthrough times. The thin first peak visible at several distances indicates that the particles in the case of high fracture transmissivity variance find relatively fast transport routes where they are experiencing

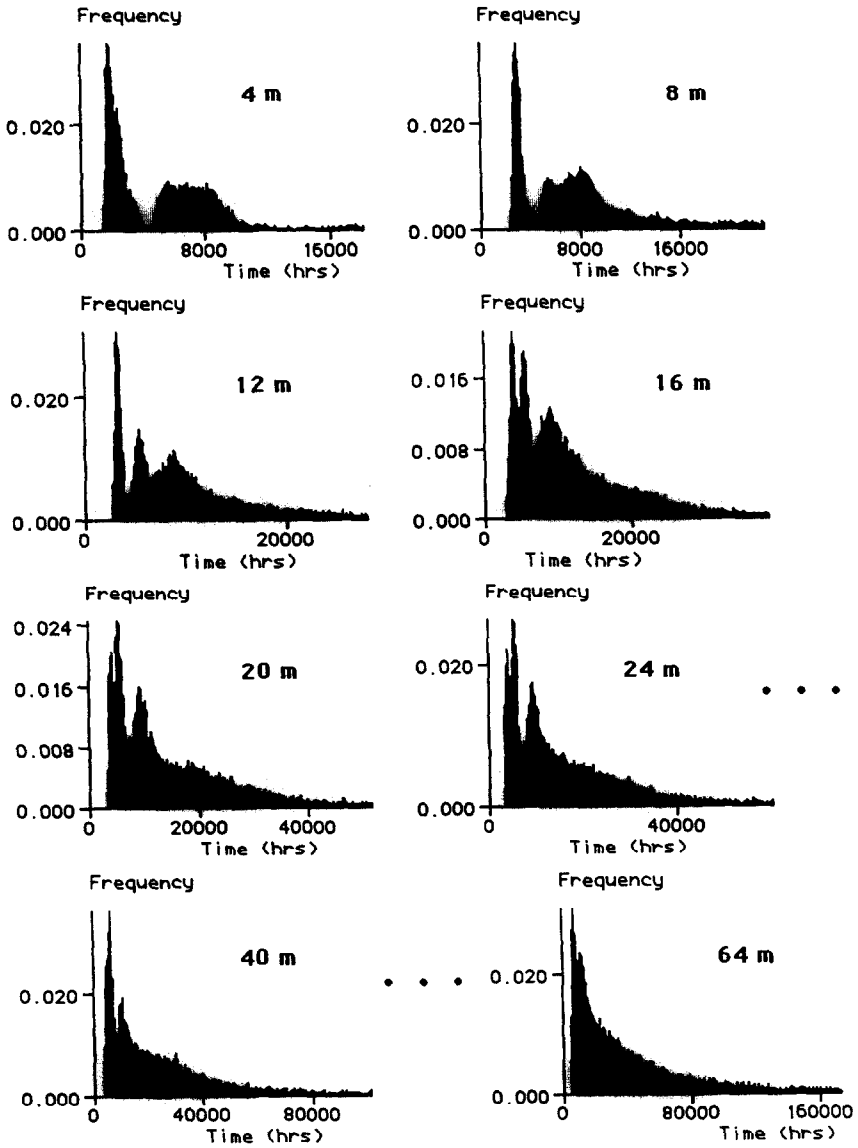

Fig. 5. A typical series of transport breakthrough curves for one realization showing relative frequency of particles vs. transport time for different distances from the source. The side of the network is 64 m and the input parameters are according to Table 1 with the high value of σ.

less dispersion (Figs. 5 and 6). Secondly, the spreading in transport time occurs on two different levels. Consider, for instance, the breakthrough curves at 4, 8 and 12 m of transport in Fig. 5. The spread within the first peak (or within any peak), the small-scale dispersion, is due to the heterogeneities within the individual fractures. The large-scale

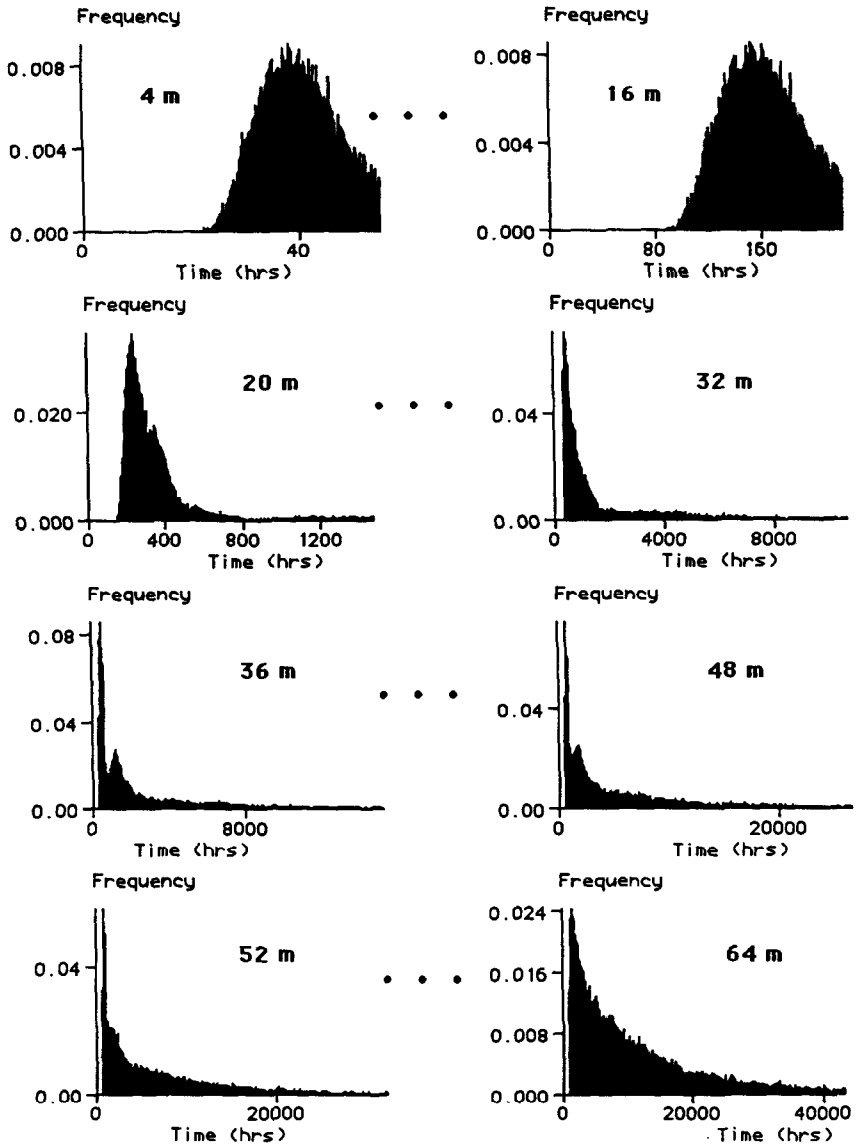

Fig. 6. A typical series of transport breakthrough curves for another realization with the same input parameters as in Fig. 5.

dispersion manifesting itself in the occurrence of more than one peak is a result of the transport taking different routes through the fracture network.

Thirdly, the larger transmissivity variance also leads to an increased number of distinguishable peaks. The appearance of more than one peak in the breakthrough curves, called multi-peak structure, at several transport distances is a common feature in field tracer experiments, conducted in fractured rock (e.g., Tsang et al., 1991). Channel-

ing, i.e. coalescence of the migrating solute in a few dominating flow paths, is assumed to be the reason for this multi-peak structure of the breakthrough curves. A simplistic assumption may then be that each peak corresponds basically to one transport route through the network. Quite frequently, however, the peaks merge and one can never be sure that what looks like a single peak in a breakthrough curve is not a superposition of two or more peaks. For this reason, the interpretation of single-peak analyses, i.e. calculations of dispersion within single peaks, is uncertain.

Finally, for a given volumetric flow rate through the network, the mean transport times are generally a few orders of magnitude longer in the high transmissivity variance cases compared to the low variance cases. The reason for this is the more frequent occurrence of large-aperture passages within the fractures for the case with the high aperture variance. In these passages the flow rate is comparatively low and, therefore, the particle residence time long.

6.2. Dispersion analysis

In heterogeneous media, there is generally a range of spatial correlation scales, so that as transport distance increases, larger correlation lengths appear and the dispersivity increases. Recent analyses of field data such as the Stripa-3D experiment, however, indicate that over a narrow range of distances the dispersion might evolve differently with transport distance along the way from the injection point to the sampling area. It has been shown using different models that dispersion in terms of Péclet number can increase or decrease (Tsang et al., 1991) with distance, or it may also be independent of transport distance (Abelin et al., 1987b).

A coefficient of variation:

$$\epsilon^{\circ} = \frac{\sigma_{1/t}}{(1/t)_{\mathrm{m}}} \tag{5}$$

where $(1/t)_{\mathrm{m}}$ is the mean of the inverted values of the transport times; and $\sigma_{1/t}$ is their standard deviation, was empirically defined for this analysis of the breakthrough curves, as a measure of the dispersion of mass in time. The inversion of the transport times reduces the otherwise strong influence on ϵ° from the tail of the mass breakthrough. The fact that early breakthrough times often are critical for performance assessment of nuclear waste repositories also motivates this way of analyzing the breakthrough curves.

The Péclet number, a measure of the dispersion in 1-D flow, is given by (Bear, 1972; Neretnieks et al., 1982):

$$\mathrm{Pe} = \frac{Lv}{D} = \frac{L}{\alpha} \tag{6}$$

where L is the transport distance; v the average flow velocity; D the dispersion coefficient; and α the dispersivity. The Péclet number may also be determined from the first and second moments of the breakthrough curve, t_m and σ_t, resepectively, as (Levenspiel, 1972):

$$\mathrm{Pe} = 2\left[\frac{t_m}{\sigma_t}\right]^2 = \frac{2}{\epsilon^2} \tag{7}$$

where ϵ is the ordinary coefficient of variation (and not based on the inverted values of the transport times).

From Eqs. 6 and 7 a measure of the dispersion length, that characterizes the size of the heterogeneities in the system, may be derived as:

$$\alpha = \frac{L\epsilon^2}{2} \tag{8}$$

As mentioned above, α would be the dispersivity if the 1-D equation describes the mass transfer. In particular, there are reasons for believing that this is the case for the individual peaks of the breakthrough curves. First, single-fracture experiments display a high degree of 1-D flow (Gentier, 1986; Bourke, 1987; INTRAVAL, 1991). Secondly, the solution to the 1-D advection–dispersion equation fits very well to the peaks of experimentally obtained breakthrough curves (Tsang et al., 1991). In this study the inverted values of the transport times are used to derive:

$$\alpha^\circ = \frac{L(\epsilon^\circ)^2}{2} \tag{9}$$

as a dispersivity measure. It is applied on the entire breakthrough as a qualitative measure of dispersion related to the heterogeneities of the system.

Generally, both experimental and modeling results of transport through discrete media display a strong dependence on scale. The present study demonstrates large variability in dispersion in terms of coefficient of variation, ϵ° (Eq. 5), up to a certain transport distance. This distance increases with the value of the fracture transmissivity variance. Figs. 7 and 8 display for individual realizations how ϵ° evolves with transport distance for the low and high fracture transmissivity variance, respectively. Ensemble means are indicated with filled circles. With the input parameters of this study, the model may produce increasing, constant or even decreasing ϵ° as a function of transport distance, i.e. individual realizations deviate substantially from the ensemble mean behavior. This irregularity is more pronounced and occurs over longer distances for the high fracture transmissivity variance, but is also discernible in the low variance case. Concurring with field observations, as mentioned in the first paragraph of this section, the transport distance dependence of tracer dispersion is indeed hard to predict. Accordingly, an important inference is that in order to characterize mass transfer from field experiments of tracer breakthrough in fractured rock one must have access to results for several different transport distances for the same tracer. Finally, due to boundary effects that are discussed in the section on spatial distribution, the results in the figures for the last 4–8 m of transport are uncertain.

Beyond a certain distance the evolution of ϵ° with transport distance tends to become more stable (Figs. 7 and 8). The reason for this is that the system gradually becomes more well-connected and behaves increasingly as a porous medium. The following discussion on dispersion length shows, however, that the porous medium approach may not be successful in explaining the tracer transport behavior.

As mentioned above, the dispersivity measure, α°, in some sense characterizes the size of the heterogeneities in the system. Fig. 9 contains the evolution of α° (as defined in Eq. 9), with transport distance. The higher values of α° for the high fracture

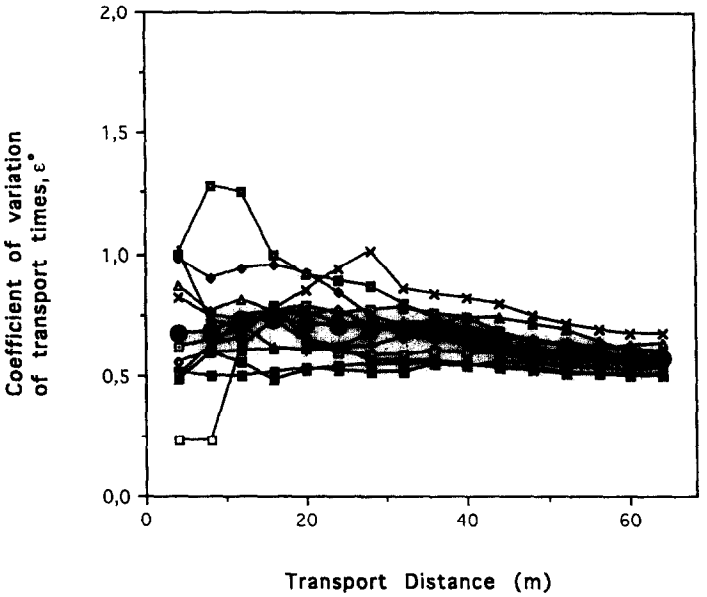

Fig. 7. Dependence of coefficient of variation, ϵ°, of the transport times on distance for the low fracture conductivity variance. The plot displays twelve realizations and the ensemble mean curve which is marked with *filled circles*.

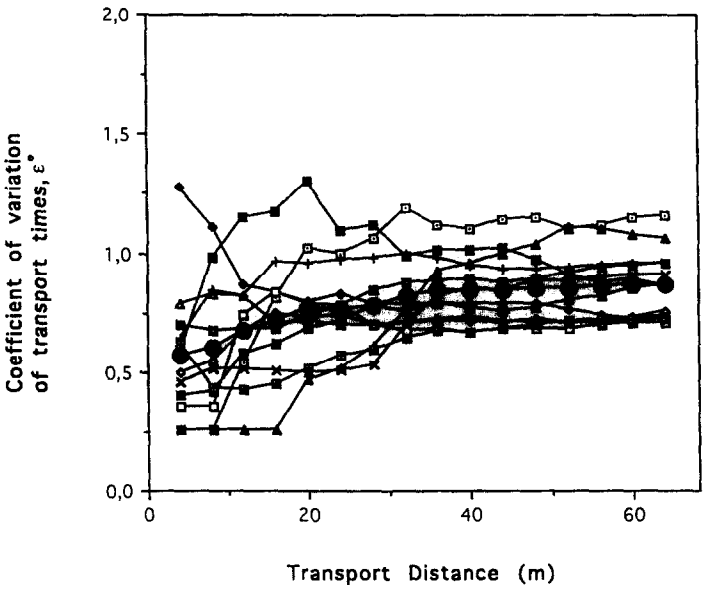

Fig. 8. Dependence of coefficient of variation, ϵ°, of the transport times on distance for the high fracture conductivity variance. The plot displays twelve realizations and the ensemble mean curve which is marked with *filled circles*.

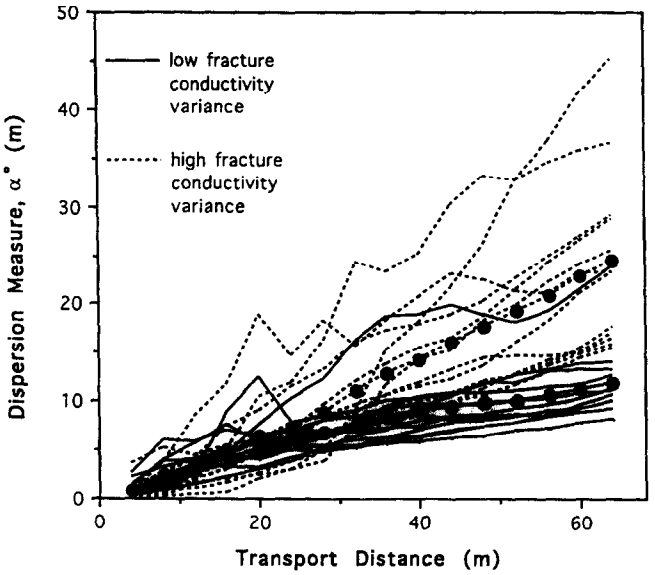

Fig. 9. Dependence of the dispersion measure, α°, on transport distance for the low and high fracture conductivity variance. The plot displays twelve realizations in each case and the ensemble mean curves which are marked with *filled circles*.

transmissivity variance (dotted curves in Fig. 9) indicate that the apparent scale of the heterogeneities is larger in the case with the high variance in fracture transmissivity. It should be noted that the twelve fracture networks were identical for the two values of fracture transmissivity variance. The apparent increase in heterogeneity scale is due to dynamic flow channeling effects. Preferential flow and transport paths run over longer distances and reduce the degree of mixing in the realizations with the high transmissivity variance.

Furthermore, α° increases with transport distance in a majority of the realizations for both values of the fracture transmissivity variance (Fig. 9). The distance dependence is much stronger for the high transmissivity variance (compare ensemble mean curves). The ensemble mean of the dispersivity measure increases linearly with transport distance without any tendency to level out. The same type of dependence has been reported from several field experiments conducted in fractured rocks (Neretnieks, 1985). Neuman (1990) presents a similar relationship from dispersivity studies using a fractal description of the hydraulic conductivity. As for the increasing α° with fracture transmissivity variance, the reason for the distance dependence of α° is network effects in terms of channeling. This explanation is consistent with earlier findings (e.g., Neretnieks, 1983) in the case of no-mixing between different flow paths.

In Fig. 9 one may also note that at distances up to ~ 20 m in a few realizations for the high fracture transmissivity variance α° is constant and much smaller than for the low variance. Here a majority of the particles are transported in just one fracture, thus experiencing only the small-scale dispersion of this single fracture. α° is therefore on

the order of the spatial correlation length in the single-fracture aperture field. As the particles travel on passing through different fractures the large-scale heterogeneities start to predominate over the small-scale heterogeneities, and α° increases.

6.3. Initial arrival time

Initial arrival time is potentially important for radionuclide migration due to radioactive decay. In the high fracture transmissivity variance case the ensemble mean of the initial arrival times are considerably higher but in occasional realizations the initial breakthrough comes earlier than in the low variance case. It is worth noting that the initial arrival times with high fracture transmissivity variance are closer to the arrival times measured in the Stripa-3D experiment. The high variability in initial arrival time is a consequence of the very irregular flow behavior that is found in the type of medium of this study. It means that any predictions about the initial breakthrough through an unknown portion of fractured rocks may be very uncertain.

6.4. Spatial distribution

The spatial distributions, i.e. the space coordinates, of the particles were registered at intermediate observation planes in the simulation domain. Figs. 10 and 11 display the particle locations by means of bars whose heights are proportional to the number of particles registered in each subarea. For the low fracture transmissivity variance (low aperture variance, Fig. 10) the mass is concentrated to a few subareas only at short transport distances. In most of these realizations an even spreading can be seen at the latest at 20 m, sometimes as early as at 12 m, without any dominant subareas. In the case with the high fracture transmissivity variance (high aperture variance, Fig. 11) this does not occur. Instead the mass is mainly concentrated to a few subareas throughout the entire transport. This agrees with the discussion on flow paths in the previous paragraph and also with field observations like the Stripa-3D experiment. It is important to note that the differences between Figs. 10 and 11 stem from different aperture variability only. The network realizations selected in these figures are identical except for the two different values of fracture aperture variance.

Finally, from Fig. 10 one also notes that at the downstream boundary there is a tendency for particles to concentrate to a few subareas for the low fracture transmissivity variance too, even though the distribution of particles in the interior of the flow domain is much more even. This is a boundary effect as flow will be directed to individual, highly conductive fractures intersecting the boundary which is maintained at a constant pressure. In the interior of the domain such highly conductive fractures often connect to low conductive fractures.

6.5. Sorption results

Figs. 12 and 13 display the breakthrough curves for the realizations corresponding to the ones in Figs. 3 and 5, but with linear sorption included. Linear sorption in combination with the low fracture transmissivity variance basically leads to a translation

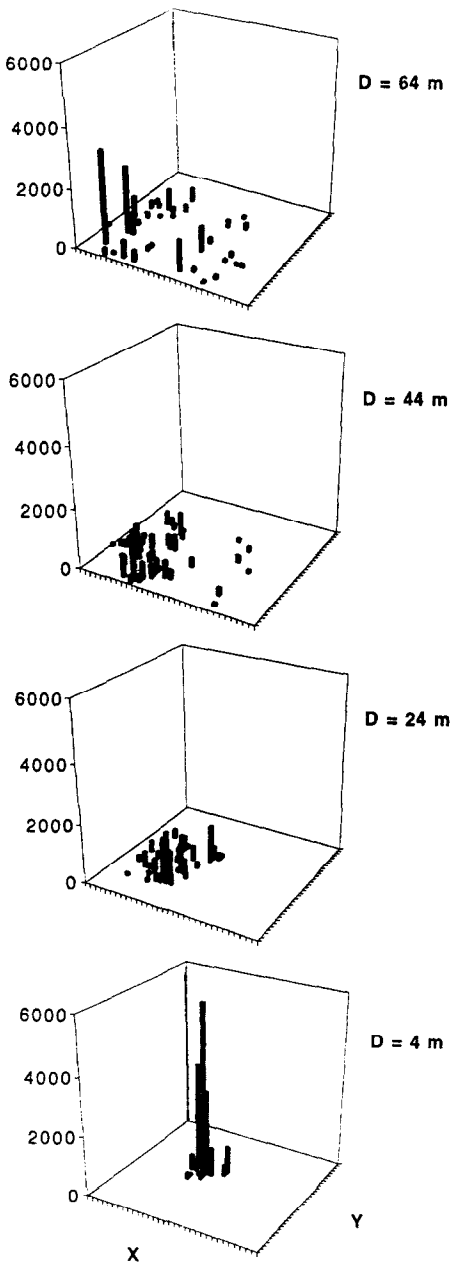

Fig. 10. Simulated tracer recovery in a fracture network realization with the low variance of fracture aperture. Each *bar* represents the recovery in a 4-m^2 sampling area. The four graphs correspond to four transport distances: 4, 24, 44 and 64 m, respectively.

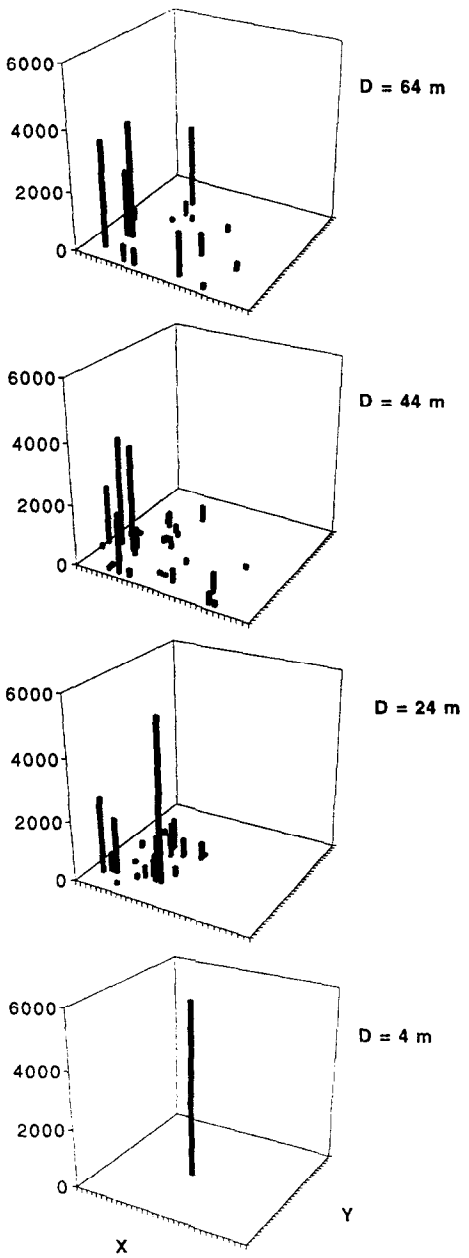

Fig. 11. Simulated tracer recovery for the same network realization as in Fig. 10 but with the high variance of fracture aperture.

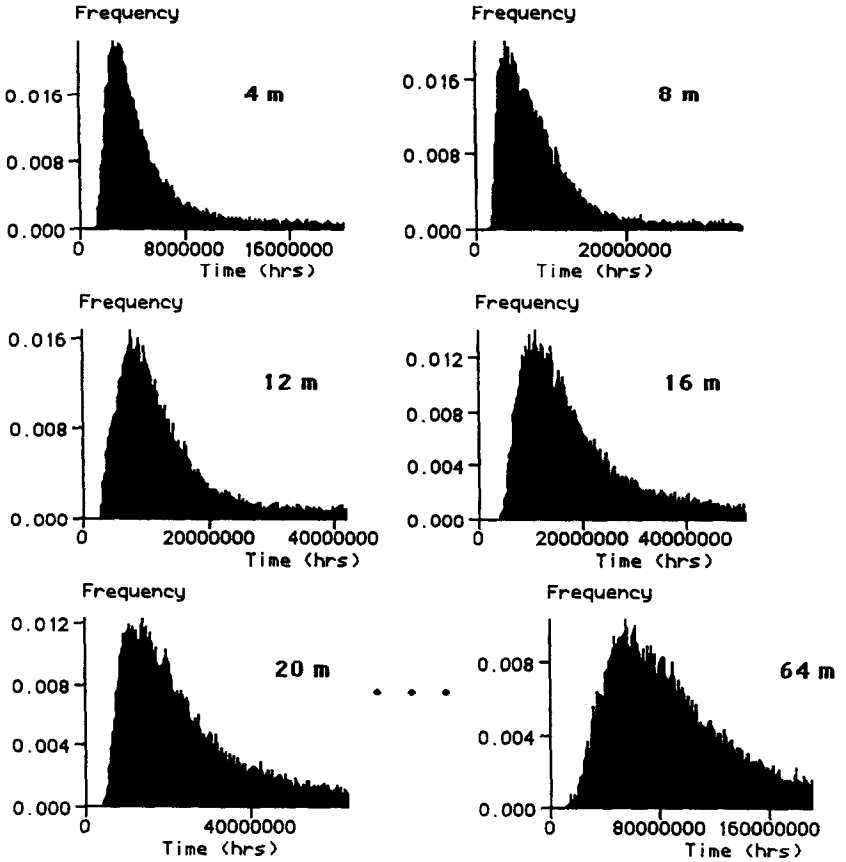

Fig. 12. A typical series of breakthrough curves at different distances from the source for the realization corresponding to Fig. 3 (low σ) but with sorbing transport.

in time of the transport (compare Figs. 3 and 12). When inspecting all 12 cases one notices that in most cases the characteristics of the curves are the same. In order to get an apprehension of the magnitude of the translation in time the relations between the mean times for non-sorbing and sorbing tracers at all transport distances is depicted in Fig. 14. The relative delay due to sorption converges toward a value of $\sim$ 27,000 which agrees well with the simplistic value (of 30,000) obtained by inserting the mean fracture aperture value, 18 μm, in Eq. 4.

For the high fracture transmissivity variance most of the peaks that were present in the non-sorption runs have merged into one smooth curve in the corresponding sorption runs (compare Figs. 5 and 13). Thus, sorption has different effect on the shape of the breakthrough curves for the low and high fracture transmissivity variance, respectively. This is expected since the variability in flow between different paths is larger with high variance; the flow field is not of the same nature as with low fracture transmissivity variance.

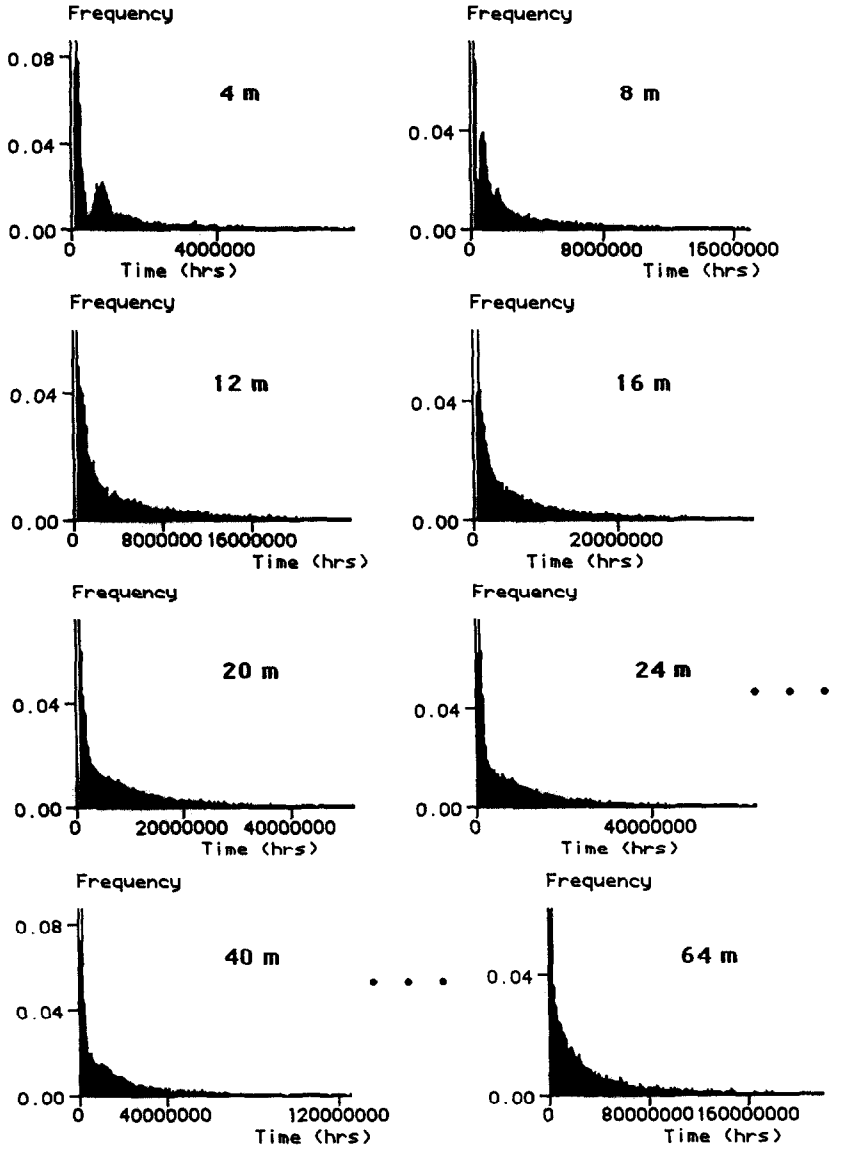

Fig. 13. A typical series of breakthrough curves at different distances from the source for the realization corresponding to Fig. 5 (high σ) but with sorbing transport.

The changes in the characteristics of the breakthrough curves imply that different fractions of the breakthrough are delayed differently. This behavior is stronger for the high variance of fracture transmissivity (fracture aperture) compared to the low variance. An investigation of all series of breakthrough curves shows that early parts of the breakthrough sometimes are delayed less than the overall transport. Furthermore, the tail

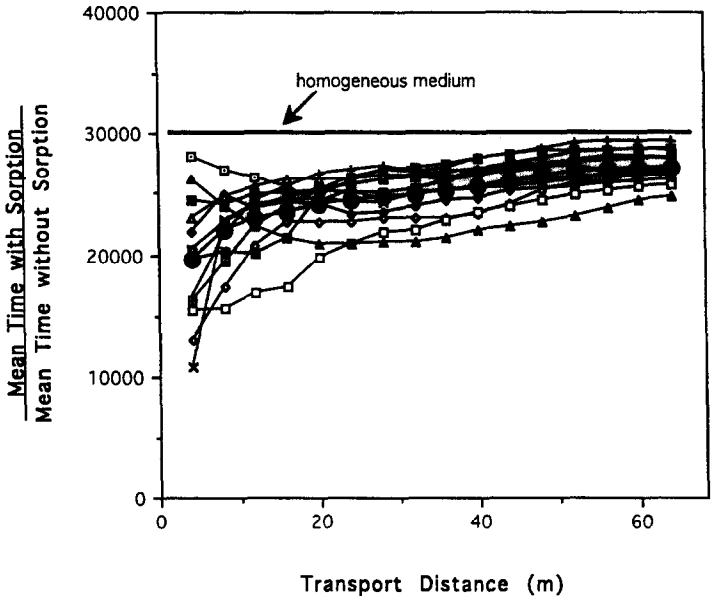

Fig. 14. Ratio between mean transport time with linear sorption (K_a equal to 270,000 m) and without linear sorption as a function of transport distance with the low fracture conductivity variance. The *horizontal line* is the theoretical value from Eq. 4.

may be substantially more delayed than the mean retardation. The reasons for these phenomena are, most certainly, that the fast particles have principally been transported in fractures or parts of fractures with large apertures where the model for linear sorption produces a small delay (Eq. 1a). On the other hand, tracers arriving late have been transported, on the average, in fractures or parts of fractures with small apertures producing large delay. The same behavior was reported by Wels and Smith (1994), using a 2-D model of parallel-plate fractures. They performed numerical transport experiments, investigating the delay due to surface sorption and concluded that the retardation of the solute plume is nonuniform and anisotropic.

The retarding effect of sorption is much less (30–50 times) in the high transmissivity variance case. The explanation can, again, be found in the structure of the flow field. There are interconnected flow paths with relatively large apertures when the single fractures are generated with the high value of fracture aperture variance. These flow paths have a smaller fracture surface area per volume of water compared to flow paths with smaller apertures. The local delay (Eq. 1a) therefore becomes smaller in a path with a large aperture, thus leading to relatively faster transport. As a result of this network effect the relation between transport times for non-sorbing and sorbing tracers does not agree with the theoretical value obtained by inserting the mean fracture aperture value, 280 μm, in Eq. 4. (See horizontal line in Fig. 15.) On the average the simulated transport time for the sorbing tracer is 2–3 times shorter compared to the value predicted by Eq. 4. Note that even though the high fracture transmissivity variance is a relatively

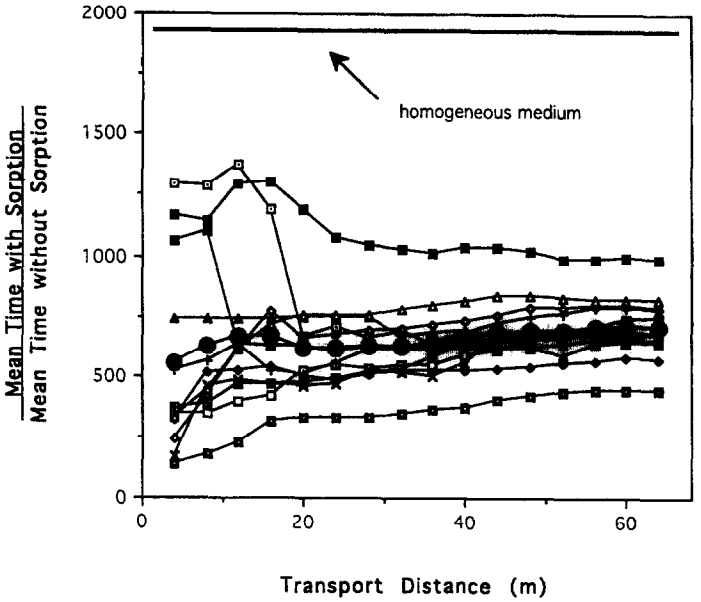

Fig. 15. Ratio between mean transport time with linear sorption (K_a equal to 270,000 m) and without linear sorption as a function of transport distance with the high fracture conductivity variance. The *horizontal line* is the theoretical value from Eq. 4.

moderate one there are occasional realizations where the delay in transport time, due to sorption, is almost one order of magnitude less than the theoretical value.

The results of the present study can be directly compared to analyses of heterogeneous porous media, where the distribution coefficient, K_d, has been assumed to be perfectly negatively correlated to the hydraulic conductivity. As an example of this, it can be noticed in Fig. 14 that, for the low variance of fracture transmissivity, the mean bulk retardation may increase with time, as was also found by Burr et al. (1994). Similarities occur principally for the low variance of fracture transmissivity due to the closer resemblance to a heterogeneous porous medium regarding the velocity field of the flow.

6.6. Geometrical parameters

The relation between the mean transport times for non-sorbing and sorbing tracer transport contains important information about the fractured medium. Inserting this relation in Eq. 4 gives an estimate of the average block grid aperture where the particles actually have been transported. For the low fracture transmissivity variance this yields a value of ~ 20 μm which is almost the same as the mean grid block aperture (of 18 μm). This implies that with the small value of fracture transmissivity variance the particles are evenly spread in the network of fractures, and thus sample the mean aperture without bias.

With the high fracture transmissivity variance the picture looks completely different. Eq. 4 gives that the transport has taken place through grid blocks with an estimated average aperture of 760 μm. This means that the particles sample an apertures that is > 150% wider than the mean aperture (of 280 μm).

An estimate of the specific surface area per volume rock, a_r, is given by:

$$a_r = a_w n \tag{10}$$

In this equation a_w is the specific surface area per volume water:

$$a_w = \frac{2}{b} \tag{11}$$

and n is the porosity which can be estimated by:

$$n = \frac{Q_{tot} t_{med}}{V} \tag{12}$$

where b is the mean fracture aperture; Q_{tot} the total flow rate; t_{med} the median transport time; and V the volume of the flow domain. Eqs. 10–12 estimate the area available to sorption per volume rock to 3.1 m^2/m^3 with low fracture transmissivity variance and to 0.8 m^2/m^3 with high variance. It is thus reduced, on an average $\sim$ 4 times, in the case with the high fracture transmissivity variance.

7. Conclusions

The transport properties of a heterogeneous discretely fractured medium differ in several aspects compared to a medium that is continuous everywhere. By means of stochastic simulations of fluid flow and solute transport several important effects of both fracture and fracture network heterogeneity have been demonstrated.

The VAPFRAC model yields multi-peak transport breakthrough curves that display dispersion on two different scales in the same way as has been reported from several field experiments. The dispersion on the larger scale is a result of the transport taking different routes through the fracture network and manifests itself by a spread-out breakthrough curve with the occurrence of more than one peak. The dispersion around each peak, the small-scale dispersion, is due to the variability in fracture aperture within the individual fractures.

In a fracture network with a high fracture transmissivity variance tracer transport tends to coalesce in a few, sparsely interconnected, pathways. This study has shown that the degree of such channeling depends on the fracture transmissivity variance. The hydraulic properties of a certain preferential pathway may deviate substantially from the medium average properties, for example in terms of dispersion. In this study, an increase in the fracture transmissivity variance by a factor of two on the natural logarithmic scale results in an increase of mean residence time with several orders of magnitude but also a small fraction of very short residence times. Furthermore, controlled by the variance of the fracture transmissivity the spatial distribution of an evolving tracer plume becomes highly irregular.

Simulations with a sorbing tracer show that the effects both in terms of relative delay and change in the characteristics of the mass breakthrough depend strongly on the degree of heterogeneity in the medium. For a high fracture transmissivity variance the simplistic relationship between mean aperture and delay due to linear sorption does not hold. There is no simple linear delay that can be described by a coefficient of retardation only. Instead, different parts of the breakthrough are delayed differently, which leads to changes in the characteristics of the curves.

The simulations illustrate how complex the process of scaling may be in fractured rocks, both going from short to longer distances and changing from conservative tracer to one that interacts with the fracture walls. Because these types of extrapolation are inevitable in the safety analysis of nuclear waste disposal, a major objective of tracer experiments should be to quantify the heterogeneity in the field, for instance in terms of transmissivity variance and correlation structure. This will provide the data necessary to evaluate complex models for flow and transport in discrete media. Since the present simulations give a plausible, physical explanation for the results of field experiments, modeling of the type presented in this paper should be a valuable tool both for analyzing combined hydraulic and tracer experiments in order to reveal heterogeneity and to make the subsequent extrapolations.

Acknowledgements

The authors of this paper are sponsored by the Swedish Nuclear Power Inspectorate (SKI), and by the Director, Office of Civilian Radioactive Waste Management, Yucca Mountain Site Characterization Office, of the U.S. Department of Energy under Contract No. DE-AC03-76SF00098. Assistance from Frank V. Hale at LBL is gratefully acknowledged.

References

Abelin, H. and Birgersson, L., 1987. 3-D migration experiment, Report 1: Site preparation and documentation. SKB (Swed. Nucl. Fuel & Waste Manage. Co.), Stockholm, Stripa Proj. Tech. Rep. 87-19.

Abelin, H., Birgersson, L. and Gidlund, J., 1987a. 3-D migration experiment, Report 2: Instrumentation and tracers. SKB (Swed. Nucl. Fuel & Waste Manage. Co.), Stockholm, Stripa Proj. Tech. Rep. 87-20.

Abelin, H., Birgersson, L., Gidlund, J., Moreno, L., Neretnieks, I., Widen, H. and Ågren, T., 1987b. 3-D migration experiment, Report 3, Part 1: Performed experiments, results and evaluation. SKB (Swed. Nucl. Fuel & Waste Manage. Co.), Stockholm, Stripa Proj. Tech. Rep. 87-21.

Abelin, H., Birgersson, L., Neretnieks, I. and Ågren, T., 1989. A channel experiment to study flow and transport in natural fractures. Proc. Conf. on Scientific Basis for Nuclear Waste Management XII, Berlin, 1988, pp. 661–668.

Andersson, J. and Dverstorp, B., 1987. Conditional simulations of fluid flow in three-dimensional networks of discrete fractures. Water Resour. Res., 23(10): 1876–1886.

Bear, J., 1972. Dynamics of Fluids in Porous Media. American Elsevier, New York, NY, 764 pp.

Black, J., Olsson, O., Gale, J. and Holmes, D., 1991. Site characterisation and validation, Stage 4: Preliminary assessment and detail prediction. SKB (Swed. Nucl. Fuel & Waste Manage. Co.), Stockholm, Stripa Proj. Tech. Rep. 91-08.

Bourke, P.J., 1987. Channeling of flow through fractures in rock. Proc. Int. GEOVAL-87 Symp., Stockholm.

Bourke, P.J., Dunance, E.M., Heath, M.J. and Hodgkinson, D.D., 1985. Fracture hydrology relevant to radionuclide transport, AERE (At. Energy Res. Establ.), Harwell, AERE Rep. 11414.

Burr, D.T., Sudicky, E.A. and Naff, R.L., 1994. Nonreactive and reactive solute transport in three-dimensional heterogeneous porous media: Mean displacement, plume spreading, and uncertainty. Water Resour. Res., 30(3): 791–815.

Cacas, M.C., Ledoux, E., de Marsily, G., Tillie, Barbreau, B.A., Durand, E., Fuega, B. and Peaudecerf, P., 1990a. Modeling fracture flow with a stochastic discrete fracture network: Calibration and validation, 1. The flow model. Water Resour. Res., 26(3): 479–489.

Cacas, M.C., Ledoux, E., de Marsily, G., Barbreau, A., Calmels, P., Gaillard, B. and Margritta, R., 1990b. Modeling fracture flow with a stochastic discrete fracture network: Calibration and validation, 2. The transport model. Water Resour. Res., 26(3): 491–500.

Cox, B.L., Preuss, K. and Persoff, P., 1989. A casting and imaging technique for determining void geometry and relative permeability behaviour of a single fracture specimen. Proc. 15th Workshop on Geothermal Reservoir Engineering, Stanford, CA.

Cvetkovic, V., 1996. Transport of reactive solutes. UNESCO (U.N. Educ. Sci. Cult. Org.) Kovacs Colloq. on Subsurface Flow and Transport: the Stochastic Approach, 26–28 Jan. 1995, Paris (in press).

Dverstorp, B., 1991. Analyzing flow and transport in fractured rock using the discrete network concept. Ph.D. Dissertation, Royal Institute of Technology, Stockholm, TRITA-VBI-151.

Dverstorp, B. and Andersson, J., 1989. Application of the discrete fracture network concept with field data: Possibilities of model calibration and validation. Water Resour. Res., 25(3): 540–550.

Dverstorp, B., Andersson, J. and Nordqvist, W., 1991. Discrete fracture network interpretation of field tracer migration in sparsely fractured rock. Water Resour. Res., 28(9): 2327-2343.

Gale, J.E., 1987. Comparison of coupled fracture deformation and fluid flow models with direct measurements of fracture pore structure and stress-flow properties. Proc. U.S. Symp. on Rock Mechanics, Tucson, AZ, pp. 1213–1222.

Gale, J.E., MacLeod, R., Strahle, A. and Carlsten, S., 1990a. Site characterisation and validation — Drift and borehole fracture data, Stage 3. SKB (Swed. Nucl. Fuel & Waste Manage. Co.), Stockholm, Stripa Proj. Tech. Rep. 90-02.

Gale, J.E., MacLeod, R. and LeMessurier, P., 1990b. Site characterisation and validation — Measurement of flowrate, solute velocities and aperture variation in natural fractures as a function of normal and shear stress, Stage 3. SKB (Swed. Nucl. Fuel & Waste Manage. Co.), Stockholm, Stripa Proj. Tech. Rep. 90-11.

Gentier, S., 1986. Morphologie et comportement hydromécanique d'une fracture naturelle dans un granite sous contrainte normale. Doctoral Thesis, Université d'Orléans, Orléans.

Hakami, E. and Barton, N., 1990. Aperture measurements and flow experiments using transparent replicas of rock joints. In: N. Barton and O. Stephansson (Editors), Rock Joints. Balkema, Rotterdam, pp. 383–390.

Hakami, E. and Stephansson, O., 1993. Experimental technique for aperture studies of intersecting joints. In: L. Ribeiro e Sousa and N.S. Grossmann (Editors), Safety and Environmental Issues in Rock Engineering, Eurock '93. Balkema, Rotterdam, pp. 301–308.

Holmes, D., Abbot, M. and Brightman, M., 1990. Site characterisation and validation — Single borehole hydraulic testing of "C" boreholes — Simulated drift experiment and small scale hydraulic testing, Stage 3. SKB (Swed. Nucl. Fuel & Waste Manage. Co.), Stockholm, Stripa Proj. Tech. Rep. 90-10.

INTRAVAL, 1991. Flow and tracer experiment in crystalline rock based on the Stripa 3-D experiment. Int. INTRAVAL Proj., Phase 1, Case 4, SKI (Swed. Nucl. Power Inspec.), Stockholm, NEA/SKI Tech. Rep.

Kent, D.B., Davis, J.A., Anderson, L.C.D., Rea, B.A. and Waite, T.D., 1994. Transport of chromium and selenium in the suboxic zone of a shallow aquifer: Influence of redox and adsorption reactions. Water Resour. Res., 30(4): 1099–1114.

Levenspiel, O., 1972. Chemical Reaction Engineering. Wiley, New York, NY, 2nd ed., 275 pp.

Long, J.C.S., Gilmour, P. and Witherspoon, P.A., 1985. A model for steady fluid flow in random three-dimensional networks of disc-shaped fractures. Water Resour. Res., 21(8): 1105–1115.

Mardia, K.V., 1972. Statistics of Directional Data. Academic Press, London.

McKinley, I.G. and Scholtis, A., 1991. Compilation and comparison of radionuclide sorption databases used in recent performance assessments. Proc. NEA (Nucl. Energy Agency) Workshop on Radionuclide Sorption from the Safety Evaluation Perspective, OECD (Org. Econ. Coop. Dev.), Paris, pp. 21–55.

Moreno, L. and Neretnieks, I., 1993a. Flow and nuclide transport in fractured media: The importance of the flow-wetted surface for radionuclide migration. In: J.I. Kim and G. de Marsily (Editors), Chemistry and Migration Behaviour of Actinides and Fission Products. J. Contam. Hydrol., 13: 49–71 (special issue).

Moreno, L. and Neretnieks, I., 1994. Fluid flow and solute transport in a network of channels. J. Contam. Hydrol., 14: 163–192.

Moreno, L. and Tsang, C.F., 1991. Multiple-peak response to tracer injection tests in single fractures: A numerical study. Water Resour. Res., 27(8): 2143–2150.

Moreno, L., Neretnieks, I. and Eriksen, T., 1985. Analysis of some laboratory tracer runs in natural fissures. Water Resour. Res., 21(7): 951–958.

Moreno, L., Tsang, Y.W., Tsang, C.F., Hale, F.V. and Neretnieks, I., 1988. Flow and tracer transport in a single fracture: A stochastic model and its relation to some field observations. Water Resour. Res., 24(12): 2033–2048.

Moreno, L., Tsang, Y.W. and Tsang, C.F., 1991. Reply. Water Resour. Res., 27(1): 133–134.

Neretnieks, I., 1983. A note on fracture flow dispersion mechanisms in the ground. Water Resour. Res., 19(2): 364–370.

Neretnieks, I., 1985. Transport in fractured rock. Mem. Int. Assoc. Hydrogeol., 17: 301–318.

Neretnieks, I., Eriksen, T. and Tähtinen, P., 1982. Tracer movement in a single fissure in granitic rock: some experimental results and their interpretation. Water Resour. Res., 18(4): 849–858.

Neuman, S.P., 1990. Universal scaling of hydraulic conductivities and dispersivities in geologic media. Water Resour. Res., 26(8): 1749–1758. 1990.

Nordqvist, A.W., Tsang, Y.W., Tsang, C.F., Dverstorp, B. and Andersson, J., 1992. A variable-aperture fracture network model for flow and transport in fractured rocks. Water Resour. Res., 28(6): 1703–1713.

Novakowski, K.S., Flavelle, P.A., Raven, K.G. and Cooper, E.L., 1985a. Determination of ground-water flow pathways in fractured plutonic rock using radioactive tracer. Int. J. Appl. Radiat. Isot., 36(5): 399–404.

Novakowski, K.S., Evans, G.V., Lever, D.A. and Raven, K.G., 1985b. A field example of measuring hydrodynamic dispersion in a single fracture. Water Resour. Res., 21(8): 1165–1174.

Ptacek, C.J. and Gillham, R.W., 1992. Laboratory and field measurements of non-equilibrium transport in the Borden aquifer, Ontario, Canada. J. Contam. Hydrol., 10: 119–158.

Rasmuson, A. and Neretnieks, I., 1986. Radionuclide transport in fast channels in crystalline rock. Water Resour. Res., 22(8): 1247–1256.

Raven, K.G., Novakowski, K.S. and Lapcevic, P.A., 1988. Interpretation of field tracer tests of a single fracture using a transient solute storage model. Water Resour. Res., 24(12): 2019–2032.

Robinson, P.C., 1986. Flow modeling in three dimensional fracture networks. Theor. Phys. Div., AERE (At. Energy Res. Establ.), Harwell, AERE Rep. R 11965.

SKI, 1991. Project-90. SKI (Swed. Nucl. Power Inspec.), Stockholm, SKI Tech. Rep. 91:23.

Stratford, G., Herbert, R.A.W. and Jackson, C.P., 1990. A parameter study of the influence of aperture variation in fracture flow and the consequences in a fractured network. In: N. Barton and O. Stephansson (Editors), Rock Joints. Balkema, Rotterdam, pp. 413–422.

Tsang, Y.W. and Tsang, C.F., 1987. Channel model of flow through fractured media. Water Resour. Res., 23(3): 467–479.

Tsang, Y.W., Tsang, C.F., Neretnieks, I. and Moreno, L., 1988. Flow and tracer transport in fractured media: A variable aperture channel model and its properties. Water Resour. Res., 24(12): 2049–2060.

Tsang, C.F., Tsang, Y.W. and Hale, F.V., 1991. Tracer transport in fractures: Analysis of field data based on a variable-aperture channel model. Water Resour. Res., 27(12): 3095–3106.

Wels, C. and Smith, L., 1994. Retardation of sorbing solutes in fractured media. Water Resour. Res., 30(9): 2547–2563.

Wikberg, P., Gustafson, G., Rhén, I. and Stanfors, R., 1991. Äspö Hard Rock Laboratory. Evaluation and conceptual modelling based on the pre-investigations 1986–1990. SKB (Swedish Nucl. Fuel & Waste Manage. Co.), Stockholm, SKB Tech. Rep. 91-22.